Characteristics of Plasma Solitons Produced by Small Orbital Debris

Alexis S. Truitt* and Christine M. Hartzell†

University of Maryland, College Park, MD 20742

October 31, 2019

Abstract

Sub-centimeter orbital debris is currently undetectable using ground-based radar and optical methods. However, the pits in Space Shuttle windows produced by paint chips (e.g. the 3.8mm diameter pit produced by a 0.2mm paint chip on STS-7) demonstrate that small debris can cause serious damage to spacecraft. Recent analytical, computational, and experimental work has shown that charged objects moving quickly through a plasma will cause the formation of plasma density solitons. Due to their exposure to the ionospheric plasma environment, even the smallest space debris will be charged. Depending on the debris size, charge and velocity, debris may produce solitons, and the plasma signature of these wave-like structures may be detected by simple instrumentation on spacecraft. Precursor solitons are of primary interest as they travel downstream ahead of the debris objects, thus allowing downstream satellites to detect an incoming debris object before collision. We will present results from computational simulations of plasma solitons generated by small orbital debris and discuss those characteristics that influence the detectability of these debris signatures. We will describe the amplitude and velocity of solitons that may be produced by mm-cm scale orbital debris in LEO. Although solitons do not dissipate in a uniform plasma environment, we will discuss the long-distance propagation of solitons through gradually varying plasma environments, in the presence of seasonal effects, diurnal effects, and damping processes, and the detectability of dissipating solitons. Plasma soliton detection would be the first collision-free method of mapping the small debris population.

1 Introduction

Sub-centimeter space debris have proven to be a threat to Earth-orbiting satellites due to their high impact velocity. For example, a 0.2 mm paint chip created a 3.8 mm diameter pit on STS-7 [1] and a millimeter sized particle which created a 40 centimeter sized crater in the Sentinel-1A solar array [2]. Yet sub-centimeter debris cannot be detected with ground based methods. Current estimates for the sub-centimeter orbital debris population are largely based on collisional detections during the Space Shuttle era. There are predicted to be more than 100 million debris objects smaller than 1 cm in diameter in Earth orbit [3, 4]. Since the Space Shuttles were retired in 2011, NASA no longer has a dedicated, calibrated orbital debris detection sensor [5, 6].

Previous work has theorized that it is possible to detect orbital debris by sensing the plasma density solitary waves, or solitons, created by the interaction of the debris with the ionospheric plasma [7, 8]. Solitons are standing waves created when nonlinear and dissipative forces are balanced. Solitons preserve their velocity and shape during translation and have a predictable wave frequency [9, 10]. Solitons are valid solutions to a variety of weakly nonlinear mathematical and physical fluid systems [11, 12, 13, 14], including space plasmas [15, 16, 17]. However, orbital debris plasma solitons have not yet been detected. Detection of debris solitons would be the first non-collisional method to map sub-centimeter orbital debris and improve the accuracy of current debris population estimates.

*Ph.D. Candidate, Department of Aerospace Engineering, 3178 Martin Hall.

†Assistant Professor, Department of Aerospace Engineering, 3178 Martin Hall.

2 Forced Korteweg-de Vries Model

The forced Korteweg-de Vries (fKdV) equation was derived to describe perturbations in the ion density due to charged debris in Earth's ionospheric plasma environment, assuming that the ions are colder than the electrons. In the absence of damping processes, the forced KdV equation is shown in Eqn 1. This derivation is covered in more detail in [18].

$$\frac{\partial \phi}{\partial \tau} + \alpha\phi\frac{\partial \phi}{\partial \xi} + \beta\frac{\partial^3 \phi}{\partial \xi^3} = \frac{1}{2}\frac{\partial f}{\partial \xi} \tag{1}$$

The nonlinear wave, U, is created by fluctuations in the electrostatic potential, ϕ. The system is normalized according to the plasma scale lengths. The spatial ξ domain is in units of the Debye length, λ_D, and the temporal domain τ is in units of Debye length divided by the ion acoustic velocity, V_{ia}, so that one time unit (TU) is λ_D/V_{ia}. The soliton wave amplitude is the perturbed ion density normalized by the unperturbed ion density, $U = (n - n_0)/n_0$. For example, a soliton with an amplitude of 1 corresponds to 2x the unperturbed ion density.

While the fKdV model assumes that solitons will propagate forever without damping in a uniform environment, Earth's ionospheric plasma is nonuniform and changes dynamically due to seasonal and diurnal effects. Additionally, ion acoustic solitary waves could interact with neutrals or electrons in the plasma, and these kinetic collisions could cause the solitons to dampen. The damped KdV (dKdV) equation, as shown in Eqn 2, has been studied for ion acoustic solitary waves in complex space plasmas with strong magnetic fields, dust, and superthermal electrons, where γ is the damping coefficient [19, 20, 21, 22]. In [23], we incorporated relevant damping processes into our precursor soliton simulations to understand the distance the solitons will propagate before complete dissipation, which will constrain detectability.

$$\frac{\partial U}{\partial \tau} + \alpha U\frac{\partial U}{\partial \xi} + \beta\frac{\partial^3 U}{\partial \xi^3} + \gamma U = \frac{1}{2}\frac{\partial f}{\partial \xi} \tag{2}$$

3 Application of fKdV to Orbital Debris

The coefficients α and β define the weighting of the steepening and dispersion terms, which drive the creation of solitons when balanced. The coefficients were derived in [18] as $\alpha = 1.0051$, and $\beta = 0.4925$, assuming a cold plasma, negligible dust density, weak magnetic field, and kappa distribution of $\kappa = 100$ [24].

[23] identified that relevant damping processes for ion acoustic waves in weakly magnetized include ion-neutral collisions and electron Landau damping [22]. However, since precursor solitons are created in plasmasphere [18], and the plasma is fully ionized [25], ion-neutral collisions have no influence on the debris precursor solitons. Since the plasmasphere is a multi-component plasma with a suprathermal tail of high energy electrons, we adopted Arshad *et al.*'s model for Landau damping [26]. In the long wavelength limit and assuming the same ion temperature, $T_{\alpha_1} = T_{\alpha_2} = T_i$, the damping rate normalized by the wave frequency, ω_r, is given as [26]:

$$\begin{aligned}\frac{\gamma}{\omega_r} = -\sqrt{\frac{\pi}{8}}\frac{\Gamma(\kappa+1)}{\Gamma(\kappa-1/2)}\frac{\sqrt{N_0^{12}}}{2^{3/2}(\kappa-1/2)^{3/2}}\Bigg[\sqrt{\frac{m_e}{m_{i1}}} + \Big(\frac{n_{0i1}}{n_{0e}}\Big)\beta_T^{3/2}\Big[1 + \frac{\beta_T N_0^{12}}{2(2\kappa-1)} + \frac{3\delta}{(2\kappa-3)N_0^{12}}\Big]^{-\kappa-1} \\ + \Big(\frac{n_{0i2}}{n_{0e}}\Big)\beta_T^{3/2}\sqrt{\frac{m_{i2}}{m_{i1}}}\Big[1 + \frac{\beta_T N_0^{12}}{2(2\kappa-1)} + \frac{3\delta}{(2\kappa-3)N_0^{12}}\frac{m_{i2}}{m_{i1}}\Big]^{-\kappa-1}\Bigg]\end{aligned} \tag{3}$$

where $\beta_T = T_e/T_i$ is the ratio of electron to ion temperature, $N_0^{12} = \Big[\frac{n_{0i1}}{n_{0e}} + \frac{n_{0i2}}{n_{0e}}\frac{m_{i1}}{m_{i2}}\Big]$, and $\delta = \Big[\frac{n_{0i1}}{n_{0e}} + \frac{n_{0i2}}{n_{0e}}(\frac{m_{i1}}{m_{i2}})^2\Big]$.

The debris force, f, in the fKdV equation is estimated as a Gaussian shape with debris radius, a, and debris velocity, V_d. The debris surface potential, due to interactions with electrons in the plasma, will create a plasma potential, Φ_p. In our normalized system, the force amplitude becomes the plasma potential divided by the electron temperature, $\Phi_{p,n}$, and the Gaussian width becomes a/λ_D [27]:

$$f(\xi, \tau) = \Phi_{p,n}\text{exp}\Big[-\Big(\frac{\xi - V_d\tau}{a/\lambda_D}\Big)^2\Big] \tag{4}$$

4 Numerical Methods

The solitons were simulated with the Chan & Kerkhoven [28] pseudospectral scheme [18], using the Fourier transform of the forcing function [9]. The final scheme was written in Matlab and applied to known analytic solutions to the fKdV [10, 27, 29], and analytic solutions to soliton damping [10]. Comparisons between the simulations and analytic solutions are provided in [18, 23].

To implement a pseudospectral scheme, the spatial domain $[-L, L]$ is discretized into N equidistant points and is normalized to $[0, 2\pi]$, so that $\Delta\xi = \frac{2\pi}{N}$ and $\xi = s(x + L)$, where $s = \frac{\pi}{L}$ so that the solution becomes periodic. The resulting normalized damped fKdV equation is:

$$\frac{\partial U}{\partial \tau} + \alpha s U \frac{\partial U}{\partial \xi} + \beta s^3 \frac{\partial^3 U}{\partial \xi^3} + \gamma U = \frac{1}{2} s \frac{\partial f}{\partial \xi} \tag{5}$$

The Chan & Kerkhoven method is recognized as the fastest method to date for solving the KdV equation [30], since it approximates the time derivative with the finite difference method, and the spatial derivatives are approximated with the leapfrog method, reducing the number of Fourier transforms required for each time step. The solution for the wave, U, then becomes:

$$U^{n+1} = \mathscr{F}^{-1}\Big[\frac{1}{1 - \Delta t \beta i s^3 k^3}((1 + \Delta t \beta i s^3 k^3)\mathscr{F}(U^{n-1}) - \Delta t \alpha i s k \mathscr{F}(U^n)^2 - \Delta t \gamma \mathscr{F}(U^n) + \Delta t i s k \mathscr{F}(f))\Big] \tag{6}$$

where $\mathscr{F}$ is the Fourier transform, $\mathscr{F}^{-1}$ is the inverse Fourier transform, and superscripts for U are in the temporal domain. Thus, $n + 1 = \tau + \Delta\tau$ and $n - 1 = \tau - \Delta\tau$.

5 Precursor Soliton Generation Criteria

In [18], we calculated that orbital debris velocity limits for creation of pinned solitons and precursor solitons. In general, pinned solitons, which travel with the debris at the same speed, are created when the debris velocity is greater than the ion acoustic velocity. Precursor solitons, which advance upstream of the debris, are created when the debris velocity is comparable to the ion acoustic velocity. Above the supercritical velocity limit, pinned solitons are produced, and below the subcritical velocity limit, no solitons are produced. In the threshold between the subcritical and supercritical velocity limits, known as the transcritical regime, precursor solitons are produced [18]. These limits can be derived by solving for the relative velocity between the force and plasma medium in Eqn 1 [9]. The supercritical and subcritical velocity limits are [9]:

$$V_{sup} = 1 + \Big(\frac{3(\alpha/2)^2 A^2}{16\beta}\Big)^{1/3} \tag{7}$$

$$V_{sub} = 1 - \Big(\frac{3(\alpha/2)^2 A^2}{4\beta}\Big)^{1/3} \tag{8}$$

where the area of the Gaussian force is [27]:

$$A = |\Phi_{p,n}|\sqrt{\pi} a/\lambda_D \tag{9}$$

6 Precursor Soliton Generation Regions

In order to identify the altitudes and latitudes where precursor solitons can be created, characteristics of the plasma environment given by the International Reference Ionosphere (IRI) model [18, 31] were used. The IRI model is hosted on NASA's Community Coordinated Modeling Center website, and characterizes the ionospheric plasma environment below 2000 km altitude. The IRI data was queried at altitudes in low Earth orbit (LEO) between 200 km - 2000 km altitude at 100 km increments, and latitudes between -90° to 90° at 10° increments, at 0° longitude. We downloaded data for two dates, July 1, 2000, and January 1, 2000 to represent plasma conditions during the summer and winter, at eight difference local times: 12am/pm, 3am/pm, 6am/pm, and 9am/pm. We created a grid of plasma parameters in

altitude, latitude, and time. For each date, there are 10,952 total grid points, with 296 grid points per altitude per date. For the plasma parameters at each grid point, we calculated orbital debris velocities that fall within the transcritical velocity limits for a given debris size. Then, we filtered the orbital debris velocities to identify orbits with eccentricities less than 1 and periapses greater than the radius of the Earth.

Soliton creation depends on the relative velocity between the ions and the orbital debris [18]. Pinned solitons, which travel with the debris at the same speed, occur when the velocity of the debris is much greater than the velocity of the ions. Pinned solitons are created in Low LEO, where the dominant ion is oxygen, since the orbital debris velocity is much higher than the ion acoustic velocity. Precursor solitons, which advance ahead of the debris, allowing for detection of the debris before collision, occur when the debris velocity is comparable to the ion acoustic velocity. Precursor solitons are created in High LEO, since the dominant ion is hydrogen and the debris velocity is comparable to the ion acoustic velocity. Typically, the transition from Low LEO to High LEO occurs at 1000 km altitude, with deviations due to seasonal and diurnal effects [25].

A subset of results are shown in Figure 1, as published in [18], for January 1, 2000, 6am UTC time, at 180° (left column) and 0° longitude (right column). The region where precursor solitons can be generated is displayed in the first row. The second row shows that this precursor generation region is limited to the area of hydrogen ion dominance. Additionally, the Debye length informs the transcritical velocity range. Shown in the third row, the electron temperature will define the ion acoustic velocity, and the ratio of the electron temperature to the ion temperature is used to calculate the damping coefficient according to Eqn 3.

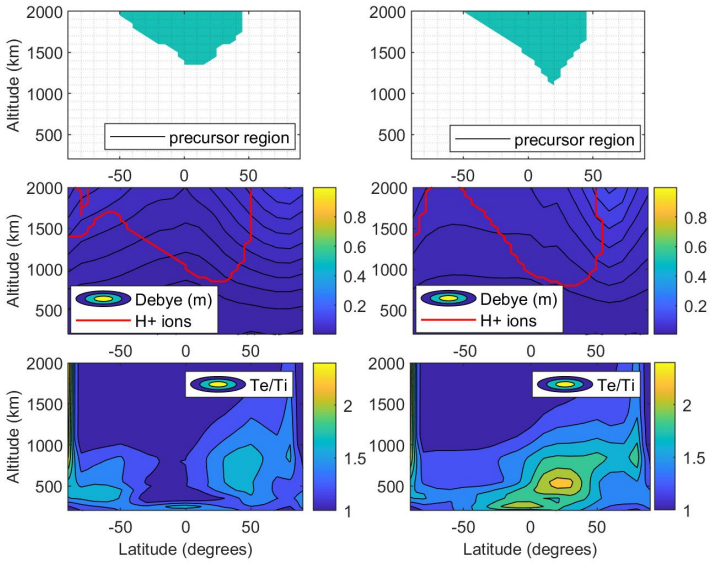

Figure 1: Precursor soliton generation region and plasma parameters for a 0.5 cm radius debris on January 1, 2000, at 6am UTC time. Left: Longitude is 180°. Right: Longitude is 0°. First row: Precursor generation region. Second row: location of the the dominant H+ ion region and the Debye length in meters. Third row: the ratio of electron temperature to ion temperature. As published in [18].

In [18], we calculated the minimum and maximum altitude and latitude where precursor solitons can be created, as shown in Figure 2, as well as the range of orbital eccentricities and the percentage of each altitude where precursor solitons can be created. For example, 28% of the grid of IRI data with 2000 km altitude and varying latitudes and local times produce precursor solitons in the summer for 0.5 cm radius debris. Considering the IRI data from the equator at 2000km altitude in the summer and varying local times, 63% of the considered longitudes and times of day produce precursor solitons for 0.5 cm radius debris. Orbital debris eccentricities for the sub-centimeter debris that produce precursor solitons ranges from $0 \leq e \leq 0.4$. Precursor solitons are more likely to be generated as the relative size between the debris and the Debye length increases. Precursor solitons can be created in the hydrogen-dominated regions by 0.5 cm radius debris down to 1000 km, 0.5 mm radius debris down to 1700 km altitude, and micron sized debris down to 1850km altitude. Additionally, the likelihood of soliton generation into medium Earth orbit (MEO),

and about other planetary bodies, is also discussed in [18].

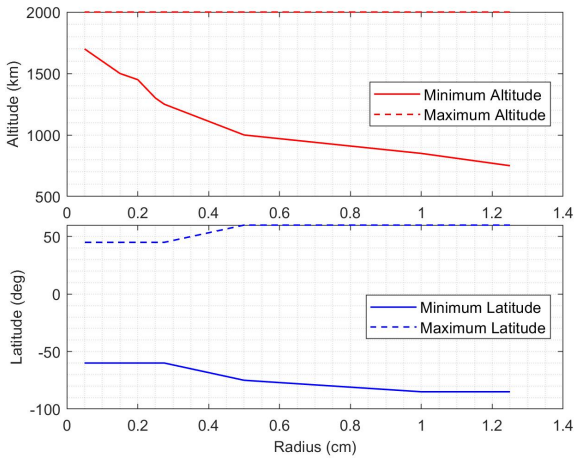

Figure 2: Minimum and maximum altitude and latitude in LEO where precursor solitons are generated as a function of debris size. The limiting altitude in the ionospheric model used is 2000 km. As published in [18].

In order to assess the feasibility of on-orbit mapping of sub-centimeter debris, models were generated to predict the soliton wave frequency, as well as the amplitude and width of precursor solitons [18]. Dimensionless 3D models were generated for undamped soliton speed, amplitude, width, and frequency as a function of debris size and velocity [18]. A total of 21 debris sizes ranging from $G = a/\lambda_D$ = 3.623 - 0.072, and 16 orbital debris velocities ranging from $V = 0.48V_{sup}$ to $1V_{sup}$ [18] were simulated, and the soliton characteristics (as a function of size and speed) were fit with biharmonic interpolation [18]. Each dimensionless debris size has its own supercritical velocity, V_{sup}. The models show that as the debris size decreases, transcritical velocity range decreases and the time to create the first precursor soliton becomes exponentially longer [18]. However, in all simulations, the time to create the first precursor soliton in High LEO is less than 10^{-2} seconds, so one can expect that debris will create precursor solitons as soon as it enters High LEO. Also, as the debris size decreases, the soliton speed and amplitude decrease, while the width increases [18]. The amplitudes of the precursor solitons fall within the range of small scale plasma irregularities frequently studied with existing sensors, including ground based radar [32], ionosondes [33], and space-based sensors [34, 35].

7 Damped Precursor Soliton Propagation Distance Prediction

Proven analytic expressions for the damping of soliton features were used to calculate the distance a precursor soliton will propagate before dissipation, considering the threshold for detection with existing sensor technology. The amplitude of small scale plasma density irregularities that can be detected is less than 0.1% of the unperturbed density [32, 33, 34, 35]. We propagate the plasma waves to the distance where the amplitude decays to 1% of the initial amplitude, which is above the current detection threshold.

In the presence of damping (γ in Eqn 2), soliton amplitude decays as $A(t) = A_0 e^{-2\gamma t/3}$, soliton speed decays as $V(t) = V_0 e^{-2\gamma t/3}$, and soliton width grows as $W(t) = W_0 e^{\gamma t/3}$ [10, 20]. The time for a soliton amplitude to decrease to 1% of its initial amplitude is:

$$t_{1\%} = \frac{3}{2}\frac{\ln(100)}{\gamma} \tag{10}$$

where $t_{1\%}$ is in units of $\omega_{pi} = V_{ia}/\lambda_D$ in our normalized coordinate system.

Next, we integrate the damped soliton speed over $t_{1\%}$ to calculate the propagation distance of a damped precursor soliton:

$$x(t_{1\%}) = \int_0^{t_{\%1}} V_0 e^{-2\gamma t/3} dt = -\frac{3}{2}\frac{V_0}{\gamma}\left(e^{-2\gamma t_{1\%}/3} - 1\right) \tag{11}$$

where V_0 is the undamped soliton speed.

Both Eqn 10 and Eqn 11 assume that solitons are propagating in an unforced system. In [23], it was demonstrated that the analytic expressions for soliton damping apply to unforced solitons and precursor forced solitons, however, pinned solitons damp at a slower rate due to the presence of a persistent force. For precursor solitons, a series of precursor solitons will be generated, and each soliton will decay according to its own lifetime.

8 Damped Precursor Soliton Simulation

The normalized damping rate γ/ω_r in Eqn 3 is calculated using the plasma parameters from the IRI model data, including the the primary and secondary ion masses and temperature, as well as the electron density and temperature. Eqn 3 is multiplied by the wave frequency, ω_r, and divided by the ion plasma frequency, ω_{pi}, so that the damping coefficient applied to the system is γ/ω_{pi} in our normalized system. The wavelength is the distance between subsequent precursor solitons, and the wave frequency is the inverse of the time between subsequent solitons, t_{12}, which depends on the force amplitude and speed. Thus, the resulting normalized wave frequency for precursor solitons in our normalized system is:

$$\omega_{r,n} = \frac{\omega_{pi}}{t_{12}} \tag{12}$$

Figure 3, as published in [23], shows an example of a precursor soliton generated from a 1 cm radius orbital debris in High LEO, in a circular orbit at 2000 km altitude. Results are shown at 500 TU for zero damping in blue and $\gamma \neq 0$ in red. IRI model data was used from July 1, 2000, 6am UTC at 0° longitude, with a Debye length of $\lambda_D = 3.63$ cm, and the ion plasma frequency of $\omega_{pi} = 1.46\text{x}10^5\ s^{-1}$. The undamped precursor soliton speed is $V_0 = 1.38V_{ia}$, and the time between precursor solitons is $t_{12} = 45.7$ TU. The wave frequency is $\omega_r = 3.7\text{x}10^3\ s^{-1}$. The normalized damping coefficient, calculated using Eqn 3, is $\gamma/\omega_r = -0.039$, with $\gamma = -9.9\text{x}10^{-4}$, and $t_{1\%} = 6.9\text{x}10^3$ TU. The propagation distance, using Eqn 11, is $x(t_{1\%}) = 405$ m.

Figure 3 also shows the analytic estimate for soliton damping. The average difference between the analytical solution and the numerical simulation for the damped soliton amplitude is 0.025, or 2% of the undamped soliton amplitude, corresponding to a density uncertainty of 531 cm^{-3} for the hydrogen ion density of $1.23\text{x}10^4$ cm^{-3} from IRI dataset. The average difference between the analytical solution and the numerical simulation for the damped soliton location is 0.013, which corresponds to a location uncertainty of 0.05 cm [23].

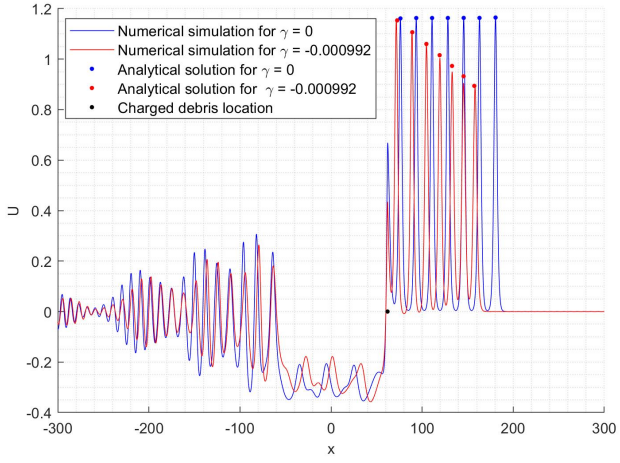

Figure 3: Precursor soliton generated by 1 cm radius orbital debris in LEO, in a circular orbit at 2000 km altitude. Results are shown at 500 TU for zero damping in blue and γ in red. As published in [23].

9 Global Model of Damped Precursor Solitons

In order to evaluate the feasibility of detecting precursor solitons with existing sensor technology, the damping coefficient Eqn 3 was used to calculate the range of propagation distances for precursor solitons in the IRI model data for High LEO, as a function of sub-centimeter debris size [23]. The damped soliton propagation distance, $x_{(t1\%)}$, depends on the undamped soliton amplitude and speed, as shown in Eqn 11. Additionally, the normalized damping coefficient, as shown in Eqn 3, depends on the ion mass, temperature, and density, as well as the soliton wave frequency. Thus, calculation of the damped propagation distance requires prior knowledge of the undamped soliton.

Using the IRI model data, the dimensionless 3D models in [18] were used to calculate the soliton wave frequency, speed, and amplitude, and the damping coefficient was calculated using the plasma parameters at each grid point [23]. Finally, the minimum, median, and maximum propagation distances, $x_{(t1\%)}$, for the damped precursor solitons was calculated as a function of debris size, as shown in Figure 4. For debris radius 0.5 mm, the minimum precursor propagation distance is 6 km, the median is 10 km, and the maximum is 49 km [23]. For each debris size, the maximum propagation distances were found in trough regions where the plasma density was lower than the surrounding regions.

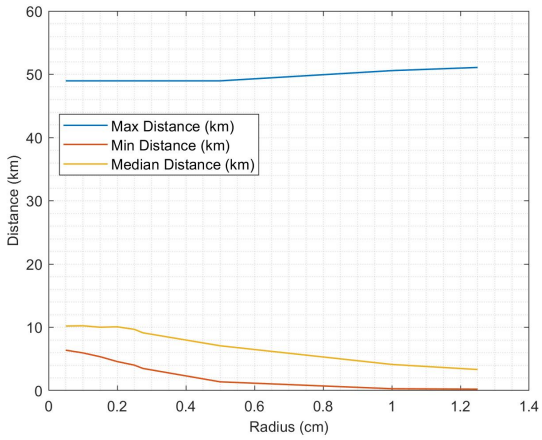

Figure 4: Minimum, median, and maximum soliton propagation distance by orbital debris size generated across all plasma environments in the IRI model data described in Section 6. As published in [23].

The likelihood that a precursor soliton will be created and propagate more than a given distance was also calculated in [23]. Figure 5 shows the percentage of IRI plasma data grid points for a given altitude where precursor solitons are created and propagate over 1 km, 5 km, and 10 km as a function of debris size according to Eqn 11, for IRI data from July 1, 2000. For example, for 0.5 mm radius debris, 20% of all latitudes at 2000 km altitude produces precursor solitons that propagate over 5 km. When considering the equator only, 50% of grid points at 2000 km altitude produce precursors for 0.5 mm radius debris that propagate over 5 km.

Since Landau damping depends on the relative temperature between the electrons and ions, seasonal and diurnal variations in the electron and ion temperature will influence propagation distance. It was shown in [23] that T_e/T_i is lower during the summer when compared to winter, and lower during the day than the night, for the mid-latitude and high altitude regions where precursor solitons can be generated. As a result, for sub-centimeter debris sizes, solitons propagate 1-2km farther in the summer when compared to winter, and day when compared to night [23].

In [23], we assessed whether the variable KdV equation [36] would be necessary to model the propagation of precursor solitons, which accounts for changing coefficients. The steepening and dispersion coefficients of the KdV equation, α and β, and will remain constant within the plasmasphere, since they are defined by the plasma's kappa-distribution in a weakly magnetized plasma. The normalized debris size, a/λ_D, and the Landau damping coefficient, γ, will also remain constant during the precursor soliton propagation distance, since the plasma parameters do not change more than 1% over the propagation distance. Therefore, variable KdV is not required to accurately model precursor soliton propagation and variations in the plasma parameters are negligible.

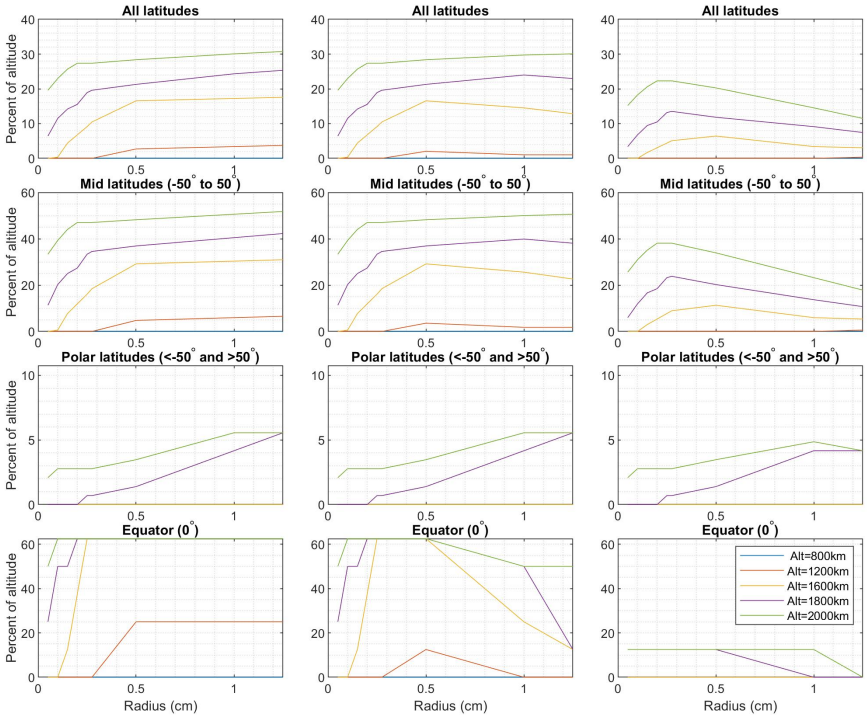

Figure 5: For July 1, 2000, the percentage of altitude in LEO where precursor solitons propagate distance is greater than 1 km (left), 5 km (center), and 10 km (right), as a function of debris size. As published in [18].

10 Conclusions and Future Work

The sub-centimeter orbital debris population is not well understood, with current estimates largely based on Space Shuttle collisional detection [3]. Ground based methods cannot detect sub-centimeter orbital debris, and are limited to high latitudes for centimeter-sized debris. In [18], we demonstrated that sub-centimeter orbital debris can create precursor solitons in High LEO, between 800 km - 2000 km altitude, where the plasma is dominated by hydrogen ions. Precursor solitons are more likely to be created at low latitudes, since the plasma density is higher when compared to high latitude regions. The amplitude, width, speed, and wave frequency of precursor solitons were modeled as a function of debris size and orbital velocity, potentially enabling the characterization of the originating debris from the precursor soliton detection [18]. Detection of precursor solitons could allow for mapping of sub-centimeter orbital debris with the first non-collisional, on-orbit method, and improve the accuracy of current debris population estimates.

While precursor solitons will not be affected by ion-neutral collisions in the fully ionized region of High LEO, they will experience Landau damping [23], which will limit the propagation distance before damping to an undetectable amplitude, driving the design of on-orbit detection constellations. The median propagation distance for precursor solitons is 10 km for 0.5 mm radius debris, and 6 km for 0.5 cm radius debris [23]. Propagation distances are influenced by seasonal and diurnal effects, with longer propagation distances during the summer when compared to winter, and day when compared to night. These propagation distances will inform the detectability of precursor solitons with ground-based or space-based detectors, the number of sensors required, and the time required to map debris. Follow on studies will extend the simulations to a 3D (2+1) environment, with two spatial dimensions and one wave amplitude dimension, to study the amplitude of the precursor soliton across the diameter of the spherical debris.

References

[1] Christiansen, E., Hyde, J., and Bernhard, R., "Space shuttle debris and meteoroid impacts," Advances in Space Research, Vol. 34, No. 5, 2004, pp. 1097–1103.

[2] Krag, H., Serrano, M., Braun, V., Kuchynka, P., Catania, M., Siminski, J., Schimmerohn, M., Marc, X., Kuijper, D., Shurmer, I., and et al., "A 1 cm space debris impact onto the Sentinel-1A solar array," Acta Astronautica, Vol. 137, Aug 2017, pp. 434–443.

[3] NASA, NASA Technology Roadmaps: TA 5: Communications, Navigation and Orbital Debris Tracking and Characterization Systems, chap. 5.7 Orbital Debris Tracking and Characterization, NASA, 2015.

[4] "NASA Orbital Debris Program Office FAQ," December 2018.

[5] Tsao, M. A., Ngo, H. T., Corsaro, R. D., and Anderson, C. R., "An In Situ Measurement System for Characterizing Orbital Debris," IEEE Transactions on Instrumentation and Measurement, Vol. 65, No. 12, Dec 2016, pp. 2758–2772.

[6] Matney, M., "NASA Orbital Debris Program Office Quarterly News," Aug 2017.

[7] Sen, A., Tiwari, S., Mishra, S., and Kaw, P., "Nonlinear wave excitations by orbiting charged space debris objects," Advances in Space Research, Vol. 56, No. 3, Aug 2015, pp. 429–435.

[8] Jaiswal, S., Bandyopadhyay, P., and Sen, A., "Experimental observation of precursor solitons in a flowing complex plasma," Physical Review E, Vol. 93, No. 4, Apr 2016.

[9] Shen, S. S., A Course on Nonlinear Waves, Springer Netherlands, 1993.

[10] Wu, T. Y.-T., "Generation of upstream advancing solitons by moving disturbances," Journal of Fluid Mechanics, Vol. 184, No. 1, Nov 1987, pp. 75.

[11] Shi, J., Xu, B., Torkar, K., Zhang, T., and Liu, Z., "An electrostatic model for nonlinear waves in the upper ionosphere," Advances in Space Research, Vol. 32, No. 3, Jan 2003, pp. 303–308.

[12] Li, X., "Synthetic aperture radar observation of the sea surface imprints of upstream atmospheric solitons generated by flow impeded by an island," Journal of Geophysical Research, Vol. 109, No. C2, 2004.

[13] Alpers, W., Wang-Chen, H., and Hock, L., "Observation of internal waves in the Andaman Sea by ERS SAR," IGARSS'97. 1997 IEEE International Geoscience and Remote Sensing Symposium Proceedings. Remote Sensing - A Scientific Vision for Sustainable Development, IEEE, 1997, pp. 1287–1292.

[14] Mitnik, L. and Dubina, V., "Spatial-temporal distribution and characteristics of internal waves in the Okhotsk and Japan Seas studied by ERS-1/2 SAR and Envisat ASAR," European Space Agency, (Special Publication) ESA SP, 07 2007.

[15] Widner, M., "Plasma Expansion into a Vacuum," Physics of Fluids, Vol. 14, No. 4, 1971, pp. 795.

[16] Lindqvist, P. A., Marklund, G. T., and Blomberg, L. G., "Plasma characteristics determined by the Freja electric field instrument," Space Science Reviews, Vol. 70, No. 3–4, Nov 1994, pp. 593–602.

[17] Trines, R., Bingham, R., Dunlop, M. W., Vaivads, A., Davies, J. A., Mendonça, J. T., Silva, L. O., and Shukla, P. K., "Spontaneous Generation of Self-Organized Solitary Wave Structures at Earth's Magnetopause," Physical Review Letters, Vol. 99, No. 20, Nov 2007.

[18] Truitt, A. S. and Hartzell, C. M., "Simulating Plasma Solitons from Orbital Debris using the Forced Korteweg–de Vries Equation (submitted)," Journal of Spacecraft and Rockets, 2019.

[19] Nouri Kadijani, M. and Zaremoghaddam, H., "Effect of Dust Grains on Dust-Ion-Acoustic KdV Solitons in Magnetized Complex Plasma with Superthermal Electrons," Journal of Fusion Energy, Vol. 31, No. 5, Nov 2011, pp. 455–462.

[20] Sultana, S., "Ion acoustic solitons in magnetized collisional non-thermal dusty plasmas," Physics Letters A, Vol. 382, No. 20, May 2018, pp. 1368–1373.

[21] Cabral, M. and Rosa, R., "Chaos for a damped and forced KdV equation," Physica D: Nonlinear Phenomena, Vol. 192, No. 3–4, Jun 2004, pp. 265–278.

[22] Ott, E., "Damping of Solitary Waves," Physics of Fluids, Vol. 13, No. 6, 1970, pp. 1432.

[23] Truitt, A. S. and Hartzell, C. M., "Simulating Damped Ion Acoustic Solitary Waves from Orbital Debris (submitted)," Journal of Spacecraft and Rockets, 2019.

[24] Pierrard, V. and Lazar, M., "Kappa Distributions: Theory and Applications in Space Plasmas," Solar Physics, Vol. 267, No. 1, Oct 2010, pp. 153–174.

[25] Prölss, G. W., Physics of the Earth's Space Environment, Springer Berlin Heidelberg, 2004.

[26] Arshad, K., Mahmood, S., and Mirza, A. M., "Landau damping of ion acoustic wave in Lorentzian multi-ion plasmas," Physics of Plasmas, Vol. 18, No. 9, Sep 2011, pp. 92115.

[27] Grimshaw, R., Maleewong, M., and Asavanant, J., "Stability of gravity-capillary waves generated by a moving pressure disturbance in water of finite depth," Physics of Fluids, Vol. 21, No. 8, Aug 2009, pp. 82–101.

[28] Chan, T. F. and Kerkhoven, T., "Fourier Methods with Extended Stability Intervals for the Korteweg-De Vries Equation," SIAM Journal on Numerical Analysis, Vol. 22, No. 3, 1985, pp. 441–454.

[29] Jun-Xiao, Z. and Bo-Ling, G., "Analytic Solutions to Forced KdV Equation," Communications in Theoretical Physics, Vol. 52, No. 2, Aug 2009, pp. 279–283.

[30] Nouri, F. and Sloan, D., "A comparison of fourier pseudospectral methods for the solution of the Korteweg-de Vries equation," Journal of Computational Physics, Vol. 83, No. 2, Aug 1989, pp. 324–344.

[31] Bilitza, D., Altadill, D., Truhlik, V., Shubin, V., Galkin, I., Reinisch, B., and Huang, X., "International Reference Ionosphere 2016: From ionospheric climate to real-time weather predictions," Space Weather, Vol. 15, No. 2, Feb 2017, pp. 418–429.

[32] Zabotin, N. A. and Wright, J. W., "Ionospheric irregularity diagnostics from the phase structure functions of MF/HF radio echoes," Radio Science, Vol. 36, No. 4, Jul 2001, pp. 757–771.

[33] Rietveld, M., Wright, J., Zabotin, N., and Pitteway, M., "The Tromsø dynasonde," Polar Science, Vol. 2, No. 1, Mar 2008, pp. 55–71.

[34] Forte, B., Coleman, C., Skone, S., Häggström, I., Mitchell, C., Da Dalt, F., Panicciari, T., Kinrade, J., and Bust, G., "Identification of scintillation signatures on GPS signals originating from plasma structures detected with EISCAT incoherent scatter radar along the same line of sight," Journal of Geophysical Research: Space Physics, Vol. 122, No. 1, Jan 2017, pp. 916–931.

[35] Sinha, H. S. S., Rocket-borne Langmuir probe for plasma density irregularities, TERRAPUB, 2013, p. 77–90.

[36] Grimshaw, R., "Internal solitary waves in a variable medium," GAMM-Mitteilungen, Vol. 30, No. 1, Apr 2007, pp. 96–109.